JOURNAL OF GEOPHYSICAL RESEARCH, VOL. 86, NO. B4, PAGES 2545–2555, APRIL 10, 1981

Geology and Seismic Structure of the Northern Section of the Oman Ophiolite

NIKOLAS I. CHRISTENSEN

Department of Geological Sciences and Graduate Program in Geophysics, University of Washington, Seattle, Washington 98195

JOHN D. SMEWING

Department of Earth Sciences, The Open University, Walton Hall, Milton Keynes, MK7 6AA, England

In the north Oman mountains, a continuous ophiolite succession is exposed, from tectonized harzburgites and dunites at the base, through layered gabbros and peridotites, high-level gabbros and plagiogranite, to a dike swarm and pillowed volcanics overlain by pelagic shales. The upper part of this sequence possesses a static metamorphic overprint, which passes downward from greenschist facies in the lowermost volcanics and most of the dike swarm to amphibolite facies in the lowermost dike swarm and in the high-level intrusives. These pervasively altered rocks are underlain by layered gabbros and peridotites, where hydration is restricted to fractures. Compressional and shear wave velocities have been measured to confining pressures of 6 kbar for 139 water-saturated cores from this sequence. The samples were field-oriented and collected from known stratigraphic levels, which allows the construction of velocity-depth profiles and an examination of anisotropy within the ophiolite. Compressional wave velocities measured for the basalt section are quite variable, ranging from 4.5 to 6.0 km/s at in situ pressures. Within the sheeted dike section, compressional and shear wave velocities vary from 5.4 to 6.3 km/s and from 2.9 to 3.6 km/s, respectively. From the basalt-sediment contact through the dike section, velocities increase rapidly with depth. This gradient is related to increasing metamorphic grade and a decrease in grain boundary porosity. The top of seismic layer 3 is located near the lower boundary of the sheeted dike swarm and marks the transition from greenschist facies to amphibolite facies metamorphics. The dikes decrease in abundance downward into the high-level intrusives: coarse-grained gabbroic and granitoid rocks, which often contain abundant hornblende, with isotropic textures and lacking compositional layering. Mean compressional and shear wave velocities increase uniformly from 6.7 and 3.6 km/s, respectively, in the high-level intrusives, to 7.5 and 3.9 km/s, respectively, at the base of the layered sequence. Measured velocities of the ultramafic tectonites are highly variable because of the anisotropy and serpentinization. Petrofabrics of relic olivine in the Wadi Ragmi region show strong preferred fabrics for the tectonites, and calculated compressional wave velocities for the serpentine-free rocks range from 7.8 to 8.5 km/s, with the fast direction parallel to the direction of spreading inferred from dike orientations, in excellent agreement with observed upper oceanic mantle seismic anisotropy. The crust-mantle boundary, which is defined by the abrupt increase in seismic velocities, coincides with the petrological contact between layered gabbros and peridotites and tectonized harzburgite and dunites.

INTRODUCTION

During the past decade, geologists and geophysicists have become considerably interested in ophiolites, because they possibly represent exposed sections of the oceanic crust and upper mantle. Since direct sampling by ocean drilling has been limited to approximately the upper 0.5 km of basalt, the most direct data presently available on much of the oceanic crust comes from marine seismic investigations, which provide information on layering and velocity distributions with depth. The seismic properties of ophiolites are thus critical in the petrologic interpretation of marine seismic refraction data.

For many of the rocks common in ophiolites, velocities as a function of pressure have been reported in several papers [e.g., *Birch,* 1960; *Christensen,* 1965, 1978; *Poster,* 1973; *Peterson et al.,* 1974; *Kroenke et al.,* 1976]. These studies have clearly established a correlation between ophiolite rock velocities and refraction velocities within the oceanic crust. Complete compressional wave and shear wave velocity profiles have recently been constructed for a traverse from the Bay of Islands ophiolite of western Newfoundland [*Salisbury and Christensen,* 1978]. This approach is particularly valuable, because it provides (1) fine crustal seismic structure, which is not presently resolvable by marine seismic techniques, for both compressional and shear waves and (2) detailed information on the petrologic nature of the seismic layers.

This paper presents compressional and shear wave velocity data at elevated pressures and petrofabric analyses for rocks from the northern portion of the Oman ophiolite. The data are used to construct seismic velocity profiles for the ophiolite. These profiles are then compared with oceanic crust and upper mantle seismic structures and with the profile from the Bay of Islands ophiolite.

The Oman ophiolite is of Turonian-Cenomanian age (95 m.y. B.P.) [*Tippit et al.,* 1981] and comprises the uppermost nappe, named the Semail nappe by *Glennie et al.* [1973], of a series of allochthonous Mesozoic thrust slices overlying the autochthonous carbonate platform of the north Arabian shield. Up to 14 km of ophiolite stratigraphy are exposed, from tectonized harzburgites and dunites at the base, through layered peridotites and gabbros, high-level gabbros and plagiogranites (the collective term for quartz diorites, tonalites and trondhjemites [*Coleman and Peterman,* 1975]), to a dike swarm and pillowed volcanics overlain by pelagic shales. The geology of the area from which most of the samples in this study were taken is shown in Figure 1, and it is represented in a cross section in Figure 2. Within this area, the ophiolite strikes uniformly N-S and dips 10°–15° to the east, as recorded by sediments within and above the pillow lavas.

Paper number 80B0924.
0148-0227/81/080B-0924$01.00

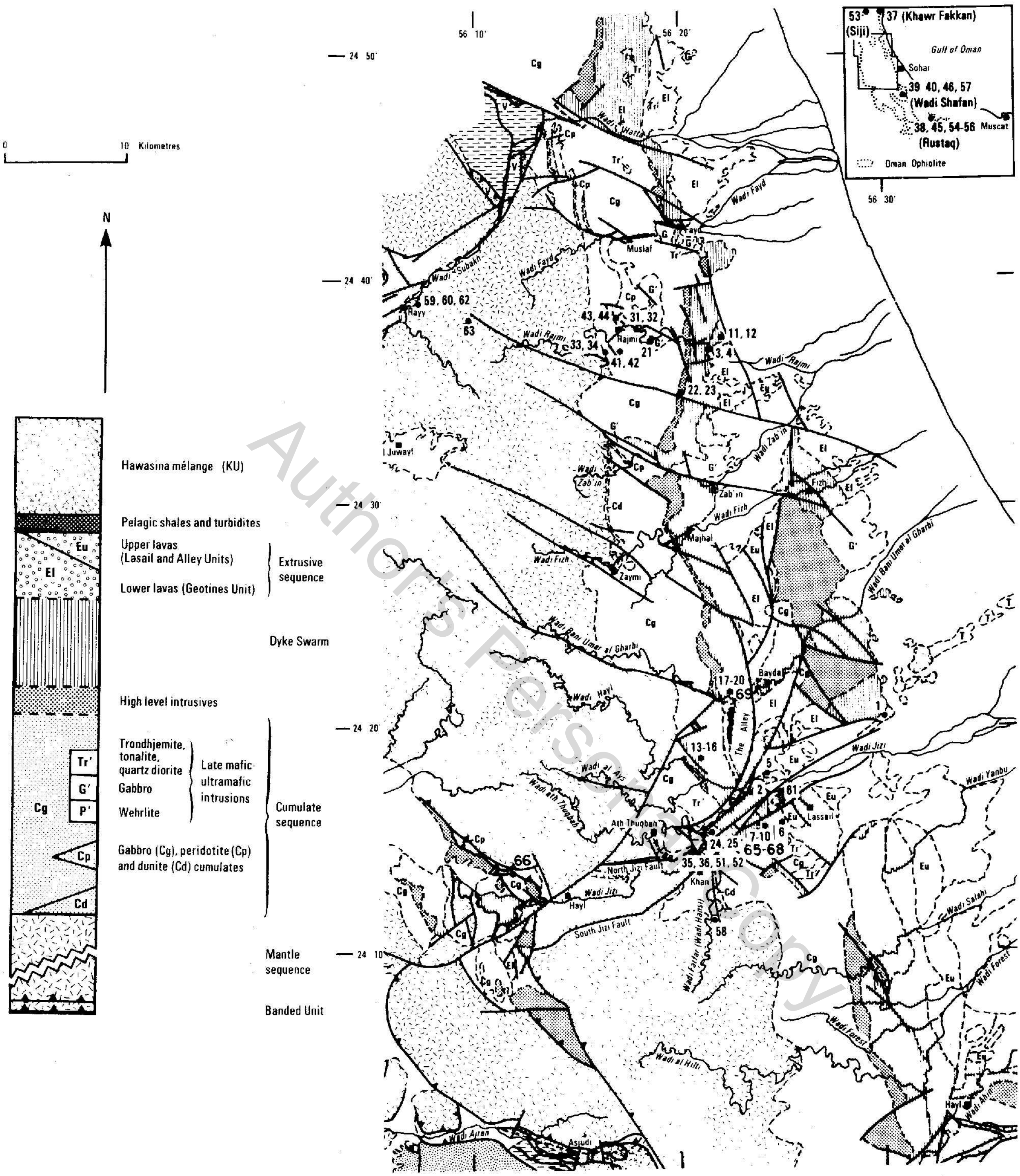

Fig. 1. Geological map of the north Oman mountains between Wadi Hata and Wadi Ahin, showing sample locations.

METHODS

Field oriented specimens were collected at known stratigraphic levels from all major units of the ophiolite (Figure 2). Sampling was carried out along traverses that were several tens of kilometers apart (Figure 1). Thus the stratigraphic section of Figure 2 and the velocity structures represent averages for over 150 km of strike. To investigate anisotropy and homogeneity, three cores with mutually perpendicular axes were taken from each sample. Core diameters ranged from 1.27 to 2.54 cm, and lengths varied from 2.5 to 6.5 cm, with the larger cores being from the coarser-grained samples. The cores were weighed when dry, then when water-saturated, and reweighed. Dry and wet bulk densities were calculated, and effective porosities were obtained from the dry and wet densities.

Each core was wrapped with 100-mesh screen and then jacketed with copper foil. The screen provides space for pore water during compression, thus maintaining relatively low pore pressures at high confining pressures. The ends of the samples were coated with silver conducting paint, electrodes and transducers were placed on the core ends, and this assembly was jacketed with gum rubber tubing to prevent the oil pressure medium from entering the rock pore spaces of the saturated samples. The velocities were measured to confining pressures of 6 kbar using the pulse transmission technique described in detail by *Birch* [1960]. Barium titanate ceramic and AC-cut quartz transducers of 2-MHz natural resonant frequencies were used to generate the compressional and shear waves, respectively.

Typical velocity data for a layered gabbro, measured at increasing and decreasing pressure, are illustrated in Figure 3. The increase in velocity with increasing pressure is primarily related to closing of pore spaces (see discussion by *Birch* [1960, 1961]). In situ pressures were estimated for each of our samples (Table 1) by using the average densities of the overlying samples and assuming 0.5-kbar confining pressure due to overlying seawater and sediments. The appropriate velocities are given in Table 1, as are water-saturated densities and Poisson's ratios calculated from mean velocities. Basalt and gabbro cores 1 and 2 were oriented parallel to the flow units and layering, and core 3 was oriented perpendicular to the planar structure.

For several of the ultramafic rocks, olivine orientation fabrics were obtained with the five-axis universal stage prior to coring. Cores for these rocks were taken with their axes parallel to maximum concentrations of olivine crystallographic *a*, *b*, and *c* axes (indicated in Table 1 by subscripts *a*, *b*, and *c*). Modal analyses of the ultramafics give serpentine contents that range from 30% to 80% by volume. The relatively low velocities for many of the ultramafics in the lower portion of the column are a consequence of this partial serpentinization, which is widely believed to originate at a late stage in the history of the ophiolite, perhaps during and after emplacement [*Christensen,* 1972; *Wenner and Taylor,* 1973]. Calculated velocities and densities for the serpentine-free rocks, based on fabric data and petrographic observations combined with single crystal data [*Christensen,* 1965; *Christensen and*

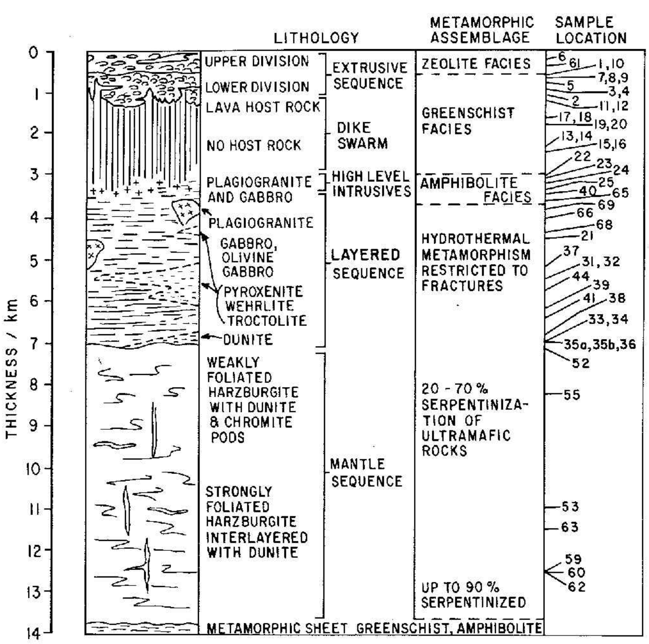

Fig. 2. Stratigraphic section of the ophiolite, showing sample depths.

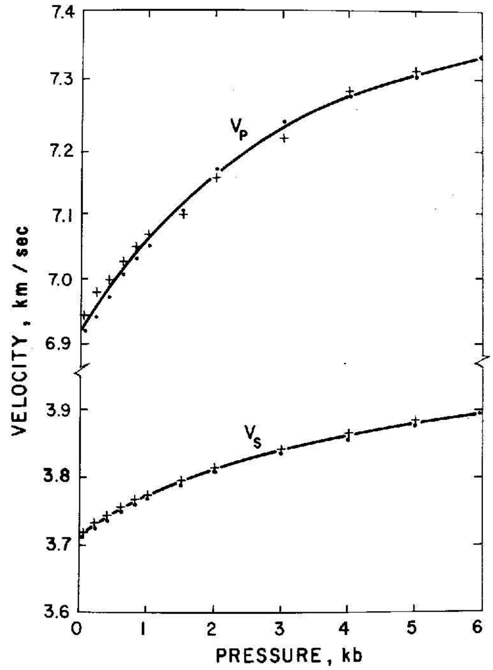

Fig. 3. Compressional V_p and shear V_s wave velocities versus pressure for gabbro 37.

Salisbury, 1979], are given in parenthesis in Table 1 for several samples within the lower ultramafic section.

VELOCITY PROFILES

Figure 4 presents the compressional and shear wave velocity data from Table 1 in their respective stratigraphic positions. Velocities for the serpentinized ultramafics are indicated as closed circles and serpentine-free velocities are shown as horizontal lines, with the lengths of the lines representing the calculated anisotropies based on petrofabric analyses. Curves showing the velocity profiles, based upon estimated relative abundances of each rock type, are shown in Figure 5. The lower portions of the curves shown in this figure are constructed for serpentine-free, isotropic rocks. Density ρ and effective porosity ϕ profiles for the ophiolite are also given in Figure 5, based again upon estimates of the relative abundances of each lithology at a given depth. These profiles are based only on the core measurements and thus do not include the influence of large-scale fracturing on the properties of the upper section. Also shown is Poisson's ratio σ calculated from the velocity profiles of Figure 5.

The profiles of Figure 5 define five distinct depth intervals, the velocities of each being related to the petrology of the ophiolite.

0–3.0 km: Pillow lavas and sheeted dike swarm. The uppermost $1\frac{1}{2}$ km of the ophiolite in this area consists of a dominantly pillowed, extrusive sequence with subordinate sheet slows, flow breccias, hyaloclastites, dikes, and sills. The extrusive sequence is divided into upper and lower units on the basis of the compositional differences of the flows [*Alabaster et al.,* 1980]. The lower unit consists of interlayered basaltic pillow lavas and sheet flows. Sheet flows often show spectacular columnar jointing, pillowed flows consist of large (1–2 m) grey-brown, poorly vesicular, aphyric lavas. The upper unit is dominantly pillowed and shows a well-developed fractionation series from basalt to rhyolite. A metamorphic facies boundary coincides with the contact between the upper and

TABLE 1. Compressional P and Shear S Wave Velocities for Samples From the Oman Ophiolite at Confining Pressures P_c Appropriate to the Sea Floor

Sample	Lithology	Depth, km	P_c, kbar	Density, g/cm³ 1	2	3	Mean	Mode	Velocity, km/s 1	2	3	Mean	Poisson's Ratio
6	Pillow lava	0.3	0.6	2.72	2.71	2.72	2.72	P	6.02	5.94	5.86	5.94	0.27
								S	3.27	3.43	3.38	3.36	
61	Pillow lava	0.4	0.6	2.61	2.63	2.59	2.61	P	5.26	5.31	4.66	5.08	0.29
								S	2.93	2.83	2.50	2.75	
1	Pillow lava	0.7	0.7	2.55	2.56	2.50	2.54	P	4.64	4.90	4.82	4.79	0.28
								S	2.39	2.67	2.85	2.64	
10	Pillow lava	0.7	0.7	2.60	2.56	2.54	2.57	P	4.80	4.95	4.81	4.85	0.33
								S	2.46	2.33	2.50	2.43	
7	Pillow lava	0.8	0.7	2.73	2.75	2.74	2.74	P	5.48	5.61	5.23	5.44	0.30
								S	2.80	3.01	2.79	2.87	
8	Pillow lava	0.8	0.7	2.63	2.66	2.71	2.67	P	5.12	5.31	5.34	5.26	0.31
								S	2.49	2.84	2.86	2.73	
9	Pillow lava	0.8	0.7	2.76	2.73	2.70	2.73	P	5.75	5.62	5.90	5.76	0.29
								S	3.08	3.06	3.12	3.09	
5	Pillow lava	0.9	0.8	2.62	2.62	2.64	2.63	P	5.76	5.91	5.63	5.77	0.31
								S	3.03	3.20	2.78	3.00	
3	Pillow lava	1.0	0.8	2.63		2.60	2.62	P	5.52		5.61	5.57	0.29
								S	3.00		3.01	3.00	
4	Pillow lava	1.0	0.8	2.61	2.59	2.58	2.59	P	4.49	5.17	4.83	4.83	0.29
								S	2.57	2.81	2.42	2.60	
2	Pillow lava	1.1	0.8	2.75	2.78	2.77	2.77	P	5.51	5.77	5.77	5.68	0.32
								S	3.00	2.66	2.96	2.87	
11	Metadolerite	1.3	0.9	2.68	2.68	2.65	2.67	P	5.61	5.42	5.41	5.48	0.28
								S	3.05	3.00	2.95	3.00	
12	Metadolerite	1.3	0.9	2.79	2.79	2.78	2.79	P	5.89	5.80	5.93	5.87	0.30
								S	3.12	3.13	3.17	3.14	
17	Metadolerite	1.8	1.0	2.73	2.72	2.73	2.73	P	5.54	5.56	5.54	5.55	0.30
								S	2.86	2.90	3.16	2.97	
18	Metadolerite	1.8	1.0	2.78	2.78	2.79	2.78	P	6.01	5.97	6.03	6.00	0.30
								S	3.21	3.17	3.17	3.18	
19	Metadolerite	1.9	1.0	2.75	2.78	2.79	2.77	P	5.74	5.77	5.76	5.76	0.29
								S	3.13	3.15	3.09	3.12	
20	Metadolerite	1.9	1.0	2.72	2.74	2.72	2.73	P	6.00	5.92	5.84	5.92	0.31
								S	3.06	3.15	3.02	3.08	
13	Metadolerite	2.4	1.2	2.78	2.80	2.79	2.79	P	6.17	6.28	6.32	6.26	0.26
								S	3.48	3.55	3.53	3.52	
14	Metadolerite	2.4	1.2	2.82	2.82	2.85	2.83	P	6.04	6.15	6.14	6.11	0.29
								S	3.16	3.39	3.30	3.28	
15	Metadolerite	2.5	1.2	2.80	2.82	2.80	2.81	P	6.07	6.22	5.98	6.09	0.30
								S	3.22	3.31	3.11	3.21	
16	Metadolerite	2.5	1.2	2.77	2.77	2.76	2.77	P	6.09	6.28	6.14	6.17	0.26
								S	3.44	3.56	3.44	3.48	
22	Trondhjemite	3.1	1.3	2.77	2.75	2.78	2.77	P	6.04	6.06	6.12	6.07	0.28
								S	3.35	3.26	3.31	3.31	
23	Metagabbro	3.2	1.4	2.97	2.92	2.89	2.93	P	7.01	7.03	6.97	7.00	0.32
								S	3.47	3.62	3.67	3.59	
24	Metagabbro	3.3	1.4	2.86	2.84	2.80	2.83	P	6.58	6.46	6.35	6.46	0.28
								S	3.45	3.54	3.66	3.55	
25	Metagabbro	3.4	1.4	2.90	2.95	2.89	2.91	P	6.80	7.01	6.92	6.91	0.28
								S	3.76	3.90	3.61	3.76	
40	Metagabbro	3.5	1.5	2.90	2.90	2.88	2.89	P	7.10	7.16	7.27	7.18	0.30
								S	3.75	3.87	3.91	3.84	
65	Metagabbro	3.6	1.5	2.87	2.82	2.82	2.84	P	6.81	6.75	6.62	6.73	0.29
								S	3.76	3.56	3.67	3.66	
69	Gabbro	3.8	1.6	2.95	2.95	2.96	2.95	P	7.22	7.08	7.07	7.12	0.28
								S	3.94	3.86	3.88	3.89	
66	Gabbro	4.2	1.7	3.00	3.01	3.02	3.01	P	7.42		7.17	7.30	0.34
								S	3.44		3.59	3.52	
68	Gabbro	4.5	1.8	2.94	2.97	2.98	2.96	P	7.37	7.34	7.16	7.29	0.28
								S	4.04	4.04	3.93	4.00	
21	Trondhjemite	4.7	1.8	2.67	2.79	2.71	2.72	P	6.23	6.50	6.20	6.31	0.26
								S	3.48	3.70	3.58	3.59	
37	Gabbro	5.3	2.0	3.02	3.04	3.06	3.04	P	7.11	7.17	7.16	7.15	0.30
								S	3.78	3.78	3.81	3.79	
31	Olivine gabbro	5.6	2.1	3.07	3.07	3.03	3.06	P	7.56	7.63	7.64	7.61	0.30
								S	4.09	4.08	3.95	4.04	
32	Olivine gabbro	5.6	2.1	3.08	3.08	3.06	3.07	P	7.55	7.75	7.75	7.68	0.31
									4.03	4.04	4.00	4.02	
44	Peridotite	5.8	2.1	3.25	3.25	3.23	3.24	P	8.09[a]	7.77[b]	7.71[c]	7.86	0.26
								S	4.47[a]	4.38[b]	4.38[c]	4.41	

TABLE 1. (continued)

Sample	Lithology	Depth, km	P_c, kbar	Density, g/cm³ 1	2	3	Mean	Mode	Velocity, km/s 1	2	3	Mean	Poisson's Ratio
39	Gabbro	6.3	2.3	3.03	2.97	3.03	3.01	P	7.42	7.38	7.35	7.38	0.30
								S	3.92	3.88	3.95	3.92	
41	Pyroxenite	6.6	2.4	3.25	3.25	3.23	3.24	P	7.81	7.73	8.27	7.94	0.27
								S	4.42	4.36	4.45	4.41	
38	Olivine gabbro	6.9	2.5	2.86	2.91	2.91	2.89	P	7.24	7.16	7.47	7.29	0.32
								S	3.75	3.61	3.86	3.74	
33	Olivine gabbro	7.0	2.5	2.92	2.94	2.95	2.94	P	6.81	7.14	7.19	7.05	0.31
								S	3.57	3.76	3.77	3.70	
34	Olivine gabbro	7.0	2.5	2.84	2.87	2.83	2.85	P	3.63	7.42	7.32	7.46	0.32
								S	3.93	3.75	3.66	3.78	
35a	Olivine gabbro	7.0	2.5	2.99	2.98	2.97	2.98	P	7.10	6.72	6.78	6.87	0.32
								S	3.63	3.31	3.62	3.52	
35b	Olivine gabbro	7.0	2.5	3.16	3.14	3.07	3.12	P	7.82	7.37	7.10	7.43	0.26
								S	4.14	4.21	4.25	4.20	
36	Olivine gabbro	7.0	2.5	3.00	3.00	2.99	2.99	P	7.42	7.57	7.41	7.47	0.31
								S	3.87	3.90	3.82	3.86	
52	Peridotite	7.2	2.5	2.88	2.81	2.87	2.85	P	6.46	6.44	6.23	6.38	0.32
								S	3.36	3.19	3.25	3.27	
55	Peridotite	8.2	2.9	2.95	2.95	2.95	2.95	P	6.74	6.84	6.52	6.70	0.31
								S	3.62	3.53	3.41	3.52	
53	Peridotite	11.0	3.8	2.78	2.76	2.79	2.78	P	6.32_a	6.00_b	6.42_c	6.25	0.31
								S	3.30_a	3.07_b	3.31_c	3.23	
63	Peridotite	11.5	3.9				(3.72)	P	(8.60)		(8.10)		
								S	(4.90)		(4.60)		
59	Peridotite	12.5	4.3				(3.32)	P	(8.60)		(8.00)		
								S	(4.80)		(4.50)		
60	Peridotite	12.5	4.3				(3.33)	P	(8.60)		(8.10)		
								S	(4.90)		(4.60)		
62	Peridotite	12.6	4.3	2.93	2.92	2.93	2.93	P	6.70_a	6.37_b	6.56_c	6.54	0.30
								S	3.53_a	3.40_b	3.53_c	3.49	

[a,b,c] Velocities were measured in directions parallel to olivine axes; concentrations based on petrofabric analyses.

lower lava units and separates zeolite facies metavolcanics above from greenschist facies metavolcanics below. In the zeolite facies lavas, partial replacement by smectite, hematite, and calcite has occurred with such zeolites as natrolite, heulandite, and laumontite being abundant in veins and amygdales. On the other hand, the greenschist facies metavolcanics show partial replacement by albite, epidote, chlorite, actinolite, sphene, pyrite, quartz, and calcite. The lack of schistosity in these rocks, the high geothermal gradient of metamorphism (greenschist facies assemblages that indicate temperatures in excess of 200°C appear at depths of less than 1 km), and the oxygen isotope data [*Gregory and Taylor,* 1980] all support an origin for these metabasalts through the circulation of seawater at a mid-ocean ridge. The extrusive sequence grades downward into the dike swarm [*Pallister,* 1981]. Within the depth interval described here, the dikes show a similar greenschist facies metamorphic assemblage to the lower lava unit.

Within this uppermost region, velocities and density increase but Poisson's ratio and porosity decrease with increasing depth (Figure 5). The velocity gradient is related to increasing metamorphic grade with depth and a decrease in grain boundary porosity. The correlation of porosity with velocity is very significant (Figure 6). In Figure 6, the mean velocity at 1 kbar for 3 cores from each sample is plotted against their mean effective porosity.

In many oceanic regions, upper crustal velocities are lowered significantly by large fractures and rubble zones within the pillow basalt and upper dike section. The presence of extensive fracturing within the upper regions of the oceanic crust has been well established through studies of the fine seismic structure of layer 2 [*Houtz and Ewing,* 1976], by basalt velocities obtained from the Deep Sea Drilling Project [*Hyndman and Drury,* 1976], and by geophysical logging within the upper few hundred meters of layer 2 [*Kirkpatrick,* 1979]. This effect has not been superimposed on the profiles of Figure 5. The actual distribution of fractures is probably quite variable, depending upon many factors, including crustal age, spreading rate, and proximity to fracture zones. The vertical extent of fracturing is also somewhat uncertain: evidence from the Oman ophiolite suggests that seawater has penetrated into the layered sequence [*Gregory and Taylor,* 1980], but metamorphic recrystallization has eliminated many of the fractures at an early stage of development.

3.0–4.0 km: Lower sheeted dike swarm and high-level intrusives. Locally, at the base of the dike swarm dense, dark green dikes occur. These contain hornblende and calcic plagioclase and represent amphibolite facies metamorphism. Texturally, these rocks are hornfelses, and it is common to find hornblende partially replacing the greenschist facies mafics, chlorite and actinolite. The textural evidence and their unique stratigraphic position suggest an origin of contact metamorphism of greenschist facies metadolerites by the intrusion of the high-level gabbros and plagiogranites into the base of the dike swarm. A similar mechanism has been proposed for amphibolite facies metadolerites in the Chilean ophiolites [*Stern et al.,* 1976]. The nature of the contact between the dike swarm and the underlying high-level intrusives (gabbros and plagiogranites) varies considerably from one section to another. Mutually intrusive relations between different members of the high-level suite are common, these contacts being obscured to varying degrees by later basaltic dikes. The overall result is

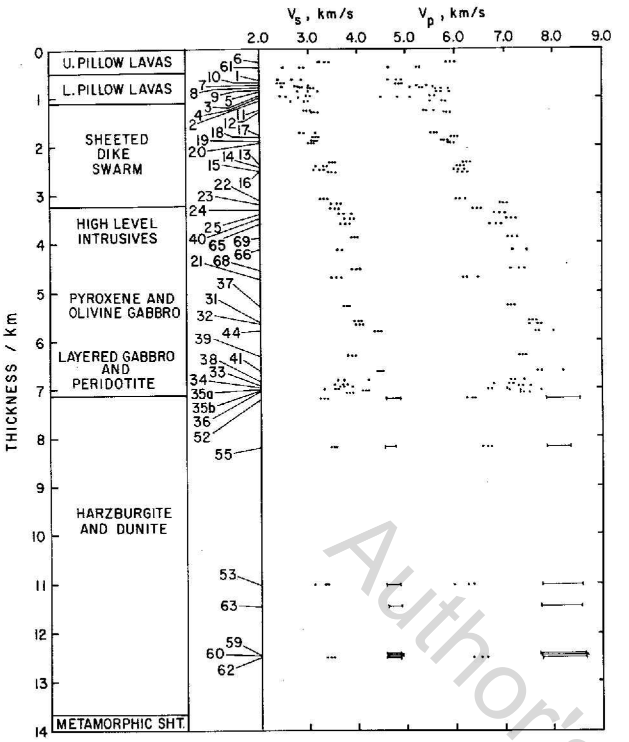

Fig. 4. Shear wave velocity V_s and compressional wave velocity V_p as a function of depth. Horizontal lines represent ranges of velocities calculated for serpentine-free ultramafics.

that dikes decrease in abundance downward until coarse-grained gabbroic and granitoid rocks that have isotropic textures and lack compositional layering are found. Olivine and pyroxene gabbros with varying amounts of primary and secondary hornblende, ferrogabbros with up to 25% modal magnetite, diorites, quartz diorities, tonalites, and trondhjemites constitute this layer, which varies in thickness from a few meters to 200 m. The intermediate members of this series are much less abundant than the basic and acidic end-members. Although most of the gabbros in this layer enclose diffuse meter-sized patches of plagiogranite, the larger plagiogranite bodies (>50 m) are localized and generally occur immediately beneath the dike swarm. All the high-level intrusives have been affected by pervasive hydrothermal alteration under upper greenschist/lower amphibolite facies conditions. Common secondary minerals include hornblende, actinolite, chlorite, epidote, clinozoisite, quartz, sphene, and sulphides.

The steep velocity gradient between 3.0 and 4.0 km depth marks this transition from greenschist facies to amphibolite facies metamorphics and correlates well with the layer 2–layer 3 seismic boundary commonly observed in oceanic crustal refraction studies. Within the Bay of Islands ophiolite the transition from layer 2 to layer 3 was also observed to coincide with the greenschist-amphibolite facies boundary [*Salisbury and Christensen, 1978*].

4.0–5.5 km: Layered sequence (upper part). With the appearance of an igneous lamination and mineral layering in the gabbros, the high-level intrusives grade rapidly downward into the layered sequence, which consists of a thick (up to 3 km) unit of interlayered gabbros and peridotites. In the upper part, peridotite layers are quite rare, most of the rocks consisting of pyroxene and olivine gabbros. Macroscopic evidence for pervasive hydrothermal metamorphism dies out with depth in this interval. However, hydrothermal circulation through this level to at least the middle part of the layered sequence is indicated by joint planes and closely spaced fracture arrays that are encrusted with secondary fibrous green hornblende. In addition, mineral δO^{18} data from layered rocks in the southern section of the ophiolite indicate that pervasive subsolidus exchange with circulating seawater has occurred to within 2 km of the base of the layered sequence [*Gregory and Taylor,* 1980]. Seawater must therefore have circulated to depths in greater than 5 km in the ophiolite crust, with the hornblende-encrusted fractures described above undoubtedly acting as hydrothermal channels.

Within this interval, seismic velocities increase with depth,

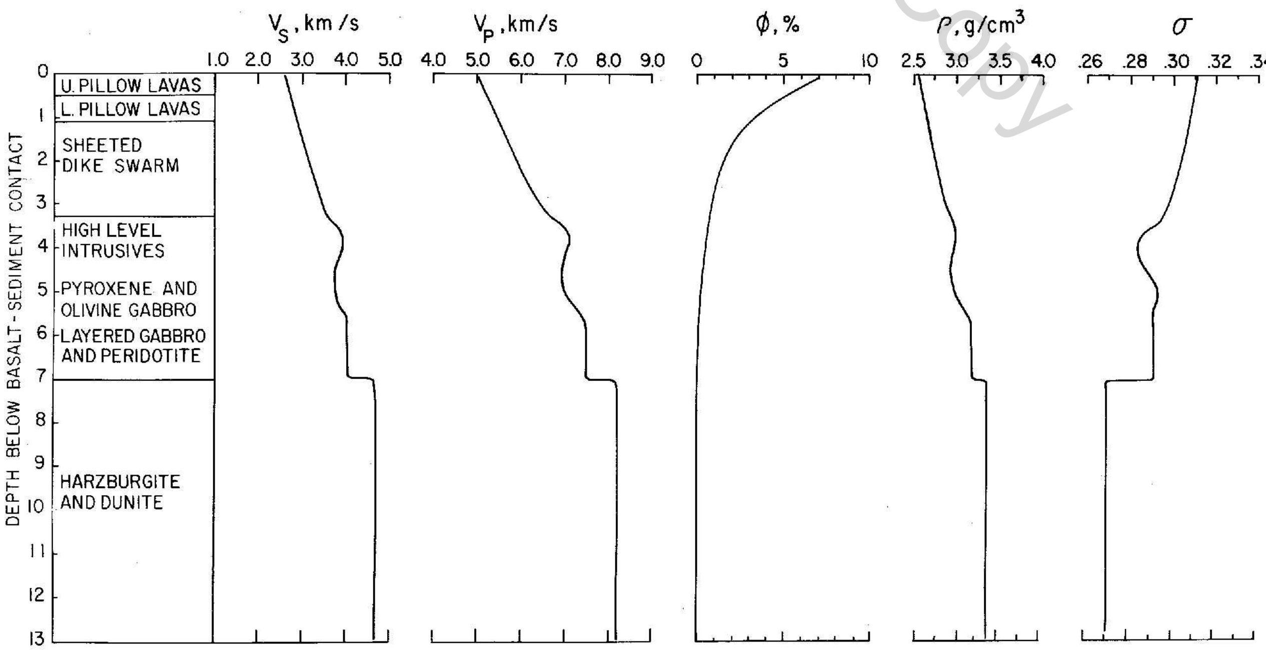

Fig. 5. Shear wave velocity V_s and compressional wave velocity V_p, effective porosity ϕ, density ρ, and Poisson's ratio σ versus depth for the northern portion of the Oman ophiolite.

consistent with increasing modal proportions of olivine and decreasing abundances of secondary minerals in the layered rocks.

5.5–7.0 km: Layered sequence (lower part). With depth, the proportion of peridotite layers (wehrlite, troctolite, pyroxenite, and dunite) to gabbroic layers increases. Velocities within this interval are quite high, usually between 6.7 and 8.3 km/s and averaging 7.5 km/s. They correlate well with the high-velocity basal layer of *Sutton et al.* [1971]. In detail, the seismic structure within this region is complex because of the interlayering on a fine scale of rocks with widely different elastic properties (Figure 4). However, with the wavelengths commonly employed in marine refraction profiles (~1.0 km), this depth region would likely be modeled as one with relatively high and uniform velocities (Figure 5).

According to our interpretation, the base of the crustal section occurs at approximately 7 km depth, in excellent agreement with average oceanic crustal thicknesses [*Raitt,* 1963; *Shor et al.,* 1971]. Beneath the layered sequence, the ultramafics are tectonized, and serpentine-free velocities are equivalent to reported upper mantle velocities. The base of the layered sequence is not invariably represented by peridotites, which is relevant to our seismic structure. In many localities, layered gabbros rest directly on the harzburgite tectonite [*Smewing,* this issue]. A particularly marked layer 3-mantle seismic discontinuity would be predicted for such sections.

7.0–13.0 km: Harzburgite and dunite. Beneath the layered sequence a unit of pervasively foliated harzburgites with minor dunites, chromitites, various coarse-grained mafic and ultramafic dikes, and a few diabase dikes is found. In keeping with interpretations of similar rocks from other ophiolites [e.g., *Malpas,* 1978], this sequence has been termed the mantle sequence, since it is regarded as the residue and melt products from partial melting of a lherzolitic mantle to form the overlying basaltic rocks. Harzburgite (80% Ol (Fo_{91}), >15% Opx (En_{91}), <5% Cpx (Wo_{45} En_{51} Fs_4) + accessory chrome spinel) constitutes 80% of the mantle sequence. The harzburgites are homogeneous on a gross scale, although a ratio segregation

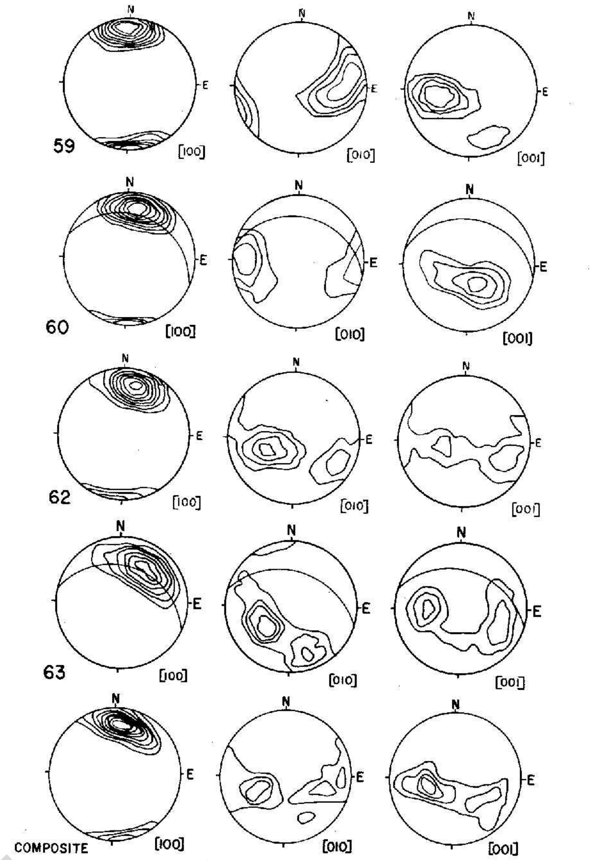

Fig. 7. Equal-area, lower-hemisphere projections of [100], [010], and [001] axes of 100 olivine grains, plotted as Kamb diagrams for samples 59, 60, 62, and 63. The projections are contoured in 2σ intervals with the lowest contour equal to 4σ. Foliation attitudes are shown for samples 60 and 62.

into more dunitic and pyroxenitic layers is ubiquitous. The foliation is generally parallel to this ratio segregation and is defined by the planar orientation of orthopyroxenes and chrome spinels. This planar orientation may also define a lineation on the foliation surfaces. Textures are porphyroclastic and granoblastic. Triple point junctions between groundmass olivines are abundant.

Lenticular bodies and anastamozing veins of dunite (Fo_{91-92} + accessory chrome spinel) occur throughout the harzburgires and lherzolites. Chromitites, exhibiting cumulate textures, are commonly associated with these dunites [*Neary and Brown,* 1979; *Brown,* 1980].

The strain state of the mantle rocks increases with depth. Harzburgites at the top of the sequence possess only a weak foliation, and dunite occurs as irregular, anastomozing dikes and veins. With increasing depth, mineral flattening and elongation become conspicuous, and the dunites occur as tabular bodies that are up to 50 m thick and 50 m in the longest dimension, parallel to the foliation plane.

The extent of serpentinization of the ultramafic rocks varies from 30% to 80%.

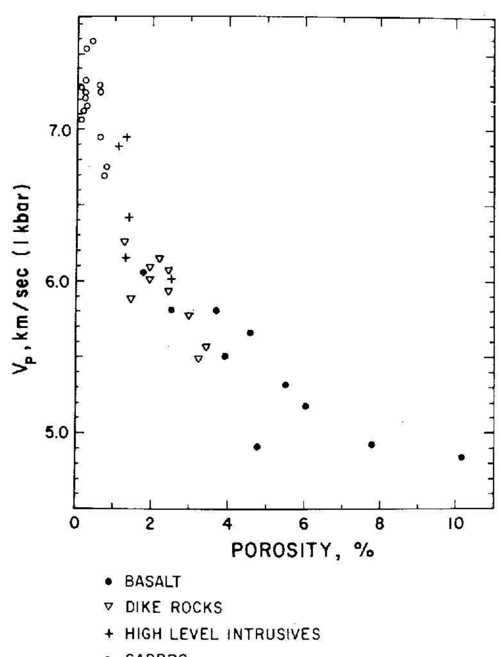

Fig. 6. Effective porosity versus mean velocity at 1 kbar.

SEISMIC ANISOTROPY WITHIN THE ULTRAMAFIC TECTONITE

The mantle harzburgite, which forms the lower 7 km of the ophiolite, can be divided on the basis of field observation into two units: the lowest 4 km generally show strongly flattened,

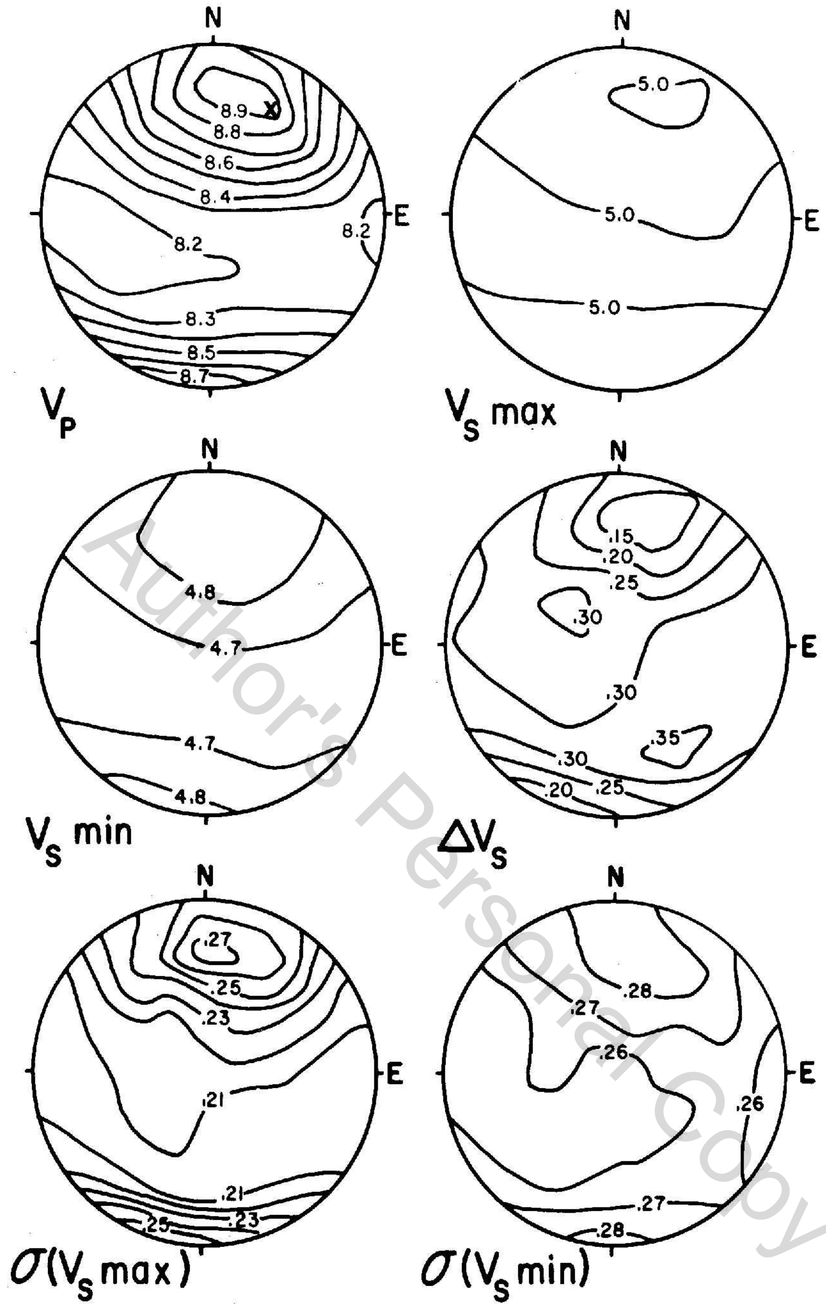

OMAN COMPOSITE

Fig. 8. Average of equal-area, lower-hemisphere projections of compressional wave velocity V_p, the maximum shear wave velocity V_s max, the minimum shear wave velocity V_s min, the shear wave dispersion ΔV_s in kilometers per second, the Poisson's ratio $\sigma(V_s$ max$)$ based on V_s max, and Poisson's ratio $\sigma(V_s$ min$)$ based on V_s min. Each projection is based on data from four samples (400 measurements). Velocity projections are contoured in 0.1-km/s intervals. The maximum concentration of projected normals to sheeted dikes within the Wadi Ragmi region is indicated by a cross in the V_p diagram.

elongate chromites and, to a lesser extent, orthopyroxene. The rocks are well foliated, and in thin section they exhibit a tectonite fabric with a preferred orientation of olivine crystallographic axes. The upper section of the harzburgite shows less evidence of strong deformation in the field; however, petrographic examination shows kinking of olivine and orthopyroxene as well as strong preferred mineral orientation. The deformation appears to be an early, high-temperature event, probably associated with stresses from mantle convective overturn beneath a spreading margin. It is not apparently associated with obduction, since the fabrics are nonparallel to obduction directions (NE to SW [*Glennie et al.*, 1973]) and the harzburgites in the lowermost 200 m of the nappe are overprinted by a lower-temperature mylonitic fabric associated with obduction, which has led to cataclasis.

Four harzburgite samples (samples 59, 60, 62, and 63) collected from the lower ultramafic section were selected for petrofabric analyses and velocity anisotropy investigations. Figure 7 illustrates olivine fabric diagrams obtained from universal stage measurements of 100 crystals from each of

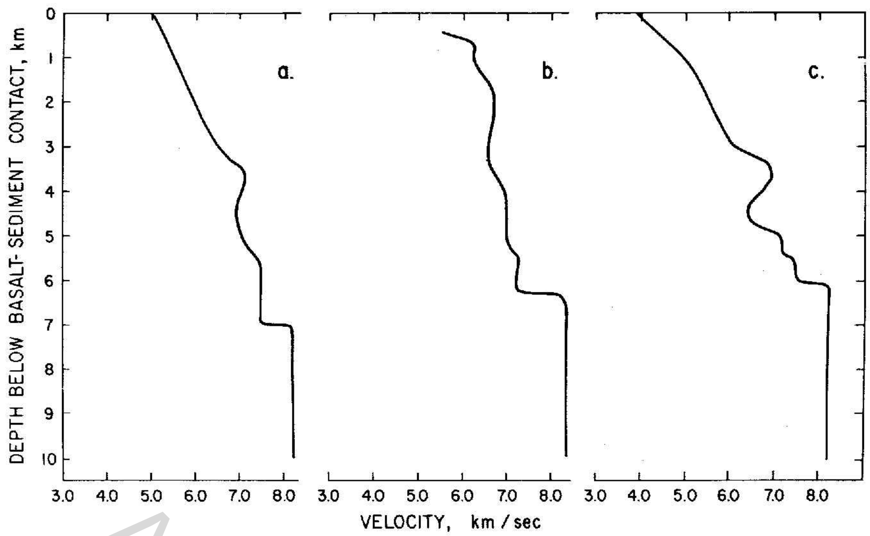

Fig. 9. Compressional wave velocity profiles for the Oman ophiolite (*a*) (Figure 5), the Blow Me Down massif, Newfoundland (*b*), and the predicted Oman profile (*c*) [*Christensen,* 1978].

these samples. Also shown is a composite diagram of the four samples. The following points are significant: (1) the preferred olivine orientation is extremely strong, especially for the olivine crystallographic *a* axes, confirming that these rocks have been deformed during a high-temperature event [*Avé Lallemant and Carter,* 1970], (2) the orientations of *a* axes are relatively constant for the four samples, dipping to the north at approximately 10°–15°, and (3) the olivine *b* and *c* axes form weaker maxima and show a tendency to form partial girdles about the *a* axes maxima.

Using the *Crosson and Lin* [1971] computer program, velocity anisotropy has been calculated at confining pressures of 2 kbar for the composite diagram in Figure 7. From the olivine fabric and single-crystal velocity data, the program calculates the contribution of each mineral to the rock velocities in specified directions. Three velocities, one compressional velocity and 2 shear velocities, are given as output for each specified propagation direction. These velocities are then contoured to show total anisotropy patterns [*Christensen and Salisbury,* 1979]. The resultant calculations are shown in Figure 8, where contours are given for compressional wave velocity V_p, the maximum shear wave velocity V_s max, the minimum shear wave velocity V_s min, the difference in shear velocities ΔV_s, Poisson's ratio calculated from V_p and V_s max, and Poisson's ratio calculated from V_p and V_s min. Several studies [e.g., *Crosson and Lin,* 1971; *Carter et al.,* 1972] have demonstrated excellent agreement between the calculated and laboratory measured velocity anisotropy.

Within anisotropic oceanic upper mantle, maximum compressional wave velocities are observed to parallel or nearly parallel spreading directions [e.g., *Raitt et al.,* 1971]. Thus if dikes within the sheeted intrusive complex form parallel to ridge crests, directions normal to the dikes should have high velocities. Such a relationship has been observed for the North Arm Massif of the Bay of Islands ophiolite [*Christensen and Salisbury,* 1979] and also appears to be the case for the Wadi Ragmi region in Oman, since the direction of maximum compressional wave velocity coincides with poles to measured dike directions (Figure 8).

DISCUSSION AND CONCLUSIONS

A major factor not recognized in earlier seismic velocity studies of ophiolites is the significant porosity in rocks from the upper section and the influence of this porosity on velocity (Figure 6). It is now apparent that grain boundary porosity at shallow depths may be as significant as large-scale fracturing in lowering seismic velocities.

Figure 9 compares the seismic velocity structure of the northern portion of the Oman ophiolite with the measured velocity structure of a traverse within the Blow Me Down Massif of the Bay of Islands ophiolite [*Salisbury and Christensen,* 1978]. Also included in the comparison is a predicted velocity profile for the Oman ophiolite [*Christensen,* 1978], based, in turn, on a stratigraphic section given by *Reinhardt* [1969]. The Bay of Islands and Oman profiles have several similarities: (1) both show rapid increases in velocities at depths appropriate for the layer 2-layer 3 boundary. In the Bay of Islands section, this boundary is within the sheeted dikes, whereas in Oman it

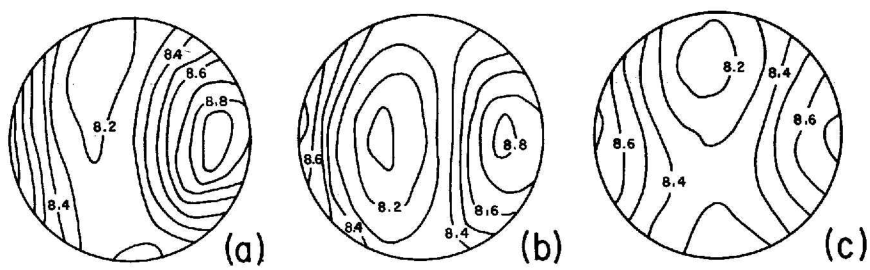

Fig. 10. A comparison of compressional wave anisotropy for peridotites from Oman (*a*), Table Mountain, Bay of Islands, Newfoundland (*b*), and North Arm Mountains, Bay of Islands, Newfoundland (*c*).

occurs near the base of the sheeted dikes, giving rise to a thicker layer 2; but for both ophiolites the top of layer 3 marks the beginning of amphibolite facies metamorphics; (2) within the upper gabbro section of both profiles, velocity inversions are likely; they are discontinuous and originate from the presence of relatively low-velocity bodies of plagiogranite [*Christensen*, 1978]; (3) a relatively high-velocity crustal basal layer (~7.5 km/s), which correlates with the high-velocity layer of *Sutton et al.* [1971], is present in both sections. In the Bay of Islands profile the high velocities are a consequence of abundant olivine gabbro, whereas in the Oman section they are produced by olivine gabbro interlayered with pyroxenite, wehrlite, troctolite, and dunite; (4) in both sections the transition from crust to mantle represents a region of predominantly mafic rocks that extend downward to tectonized harzburgite. For both ophiolites the mafic crustal sections are similar in thickness to average sections determined by refraction techniques. It is therefore not necessary to add serpentinized ultramafic to the mafic sections in order to produce reasonable crustal thickness, as suggested by *Clague and Straley* [1977]; (5) the magnitude and symmetry of compressional wave seismic anisotropy within the Oman ophiolite are similar to those of the Bay of Islands ophiolite (Figure 10). For comparison with oceanic upper-mantle refraction data, the absolute velocities of both diagrams should be lowered by approximately 0.4 km/s because of temperature effects and the presence of orthopyroxene [*Christensen and Salisbury*, 1979]. Thus the magnitude of the velocities (7.8–8.5 km/s) and the anisotropy (8%), as well as the direction of maximum velocity inferred from the dike orientations, agree well with seismic studies of compressional wave velocities in the oceanic upper mantle [*Raitt et al.*, 1971].

In summary, we conclude that the seismic structure of the Oman ophiolite is remarkably similar to that of the oceanic crust and upper mantle. Important differences, likely to be observed as different oceanic seismic structures, do exist between ophiolites. Nevertheless, the overall structures are quite similar, and it is thus possible to observe directly in ophiolites the petrologic features that are responsible for oceanic crustal and upper mantle seismic structure.

Acknowledgments. We wish to thank S. Blair, S. Lundquist, L. Slater, and R. Wilkens for their assistance in obtaining the velocity data, the Department of Petroleum and Minerals, Muscat, particularly M. Kassim and Dr. I. M. Elboushi for help in Oman, and M. A. Brown, P. Browning and Dr. S. J. Lippard for helpful comments on a first draft of this manuscript. This investigation was supported by the Office of Naval Research contract N-00014-75-C-0592 and the National Environment Research Council, Great Britain.

REFERENCES

Alabaster, T., J. A. Pearce, D. I. J. Mallick, and I. M. Elboushi, The volcanic stratigraphy and location of massive-sulphide deposits in the Oman ophiolite, in *International Ophiolite Symposium, Nicosia, Cyprus,* Geological Survey Department, Nicosia, Cyprus, 1980.

Avé Lallemant, H. G., and N. L. Carter, Syntectonic recrystallization of olivine and modes of flow in the upper mantle, *Geol. Soc. Am. Bull., 81,* 2203–2220, 1970.

Birch, F., The velocity of compressional waves in rocks to 10 kilobars, 1, *J. Geophys. Res., 65,* 1083–1102, 1960.

Birch, F., The velocity of compressional waves in rocks to 10 kilobars, 2, *J. Geophys. Res., 66,* 2199–2224, 1961.

Brown, M. A., Textural and geochemical evidence for the origin of some chromite deposits in the Oman ophiolite, in *International Ophiolite Symposium, Nicosia, Cyprus,* Geological Survey Department, Nicosia, Cyprus, 1980.

Carter, N. L., D. W. Baker, and R. P. George, Jr., Seismic anisotropy, flow and constitution of the upper mantle, in *Flow and Fracture of Rocks, Geophys. Monogr. Ser.,* vol. 16, edited by H. C. Heard, I. Y. Borg, N. L. Carter, and C. B. Raleigh, pp. 167–190, AGU, Washington, D. C., 1972.

Christensen, N. I., Compressional wave velocities in metamorphic rocks at pressures to 10 kilobars, *J. Geophys. Res., 70,* 6147–6164, 1965.

Christensen, N. I., The abundance of serpentinites in the ocean crust, *J. Geol., 80,* 709–719, 1972.

Christensen, N. I., Ophiolites, seismic velocities and oceanic crustal structure, *Tectonophysics, 47,* 131–157, 1978.

Christensen, N. I., and M. H. Salisbury, Seismic anisotropy in the oceanic upper mantle: Evidence from the Bay of Islands ophiolite complex, *J. Geophys. Res., 84,* 4601–4610, 1979.

Clague, D. A., and P. F. Straley, Petrologic nature of the oceanic Moho, *Geology, 5,* 133–136, 1977.

Coleman, R. G., and Z. E. Peterman, Oceanic plagiogranite, *J. Geophys. Res., 80,* 1099–1108, 1975.

Crosson, R. S., and J. W. Lin, Voight and Reuss prediction of anisotropic elasticity of dunite, *J. Geophys. Res., 76,* 570–578, 1971.

Glennie, K. W., M. G. A. Boeuf, M. W. Hughes-Clarke, M. Moody-Stuart, W. F. H. Pilaar, and B. M. Reinhardt, Late Cretaceous nappes in Oman mountains and their geologic evolution, *Am. Assoc. Petrol. Geol. Bull., 57,* 5–27, 1973.

Gregory, R. T., and H. P. Taylor, O^{18}/O^{16} variations in gabbro, diabase and volcanic sections in the Samail ophiolite, southeastern Oman mountains and the nature of hydrothermal alteration in the oceanic crust, in *International Ophiolite Symposium, Nicosia, Cyprus,* Geological Survey Department, Nicosia, Cyprus, 1980.

Houtz, R., and J. Ewing, Upper crustal structure as a function of plate age, *J. Geophys. Res., 81,* 2490–2498, 1976.

Hyndman, R. D., and M. Drury, The physical properties of oceanic basement rocks from deep sea drilling on the Mid-Atlantic Ridge, *J. Geophys. Res., 81,* 4042–4052, 1976.

Kirkpatrick, R. J., The physical state of the oceanic crust: Results of downhole geophysical logging in the Mid-Atlantic Ridge at 23°N, *J. Geophys, Res., 84,* 178–188, 1979.

Kroenke, L. W., M. H. Manghnani, C. S. Rai, P. Fryer, and R. Ramananantoandro, Elastic properties of selected ophiolite rocks from Papua, New Guinea: Nature and composition of oceanic lower crust and upper mantle, in *The Geophysics of the Pacific Ocean Basin and Its Margin, Geophys. Monogr. Ser.,* vol. 19, edited by G. H. Sutton, M. H. Manghnani, and R. Moberly, pp. 407–421, AGU, Washington, D. C., 1976.

Malpas, J. G., Magma generation in the upper mantle, field evidence from ophiolite suites and application to the generation of oceanic lithosphere, *Phil. Trans. Roy. Soc. London, Ser. A, 288,* 527–546, 1978.

Neary, C. R., and M. A. Brown, Chromites from the Al'Ays Complex, Saudi Arabia and the Semail Complex, Oman, Evolution and Mineralization of the Arabian Shield, edited by A. M. S. Al-Shanti, *I. A. G. Bull., 2,* 193–205, 1979.

Pallister, J. S., Structure of the sheeted dike complex of the Samail ophiolite near Ibra, Oman, *J. Geophys. Res., 86,* this issue, 1981.

Peterson, J. J., P. J. Fox, and E. Schreiber, Newfoundland ophiolites and the geology of the oceanic layer, *Nature, 247,* 194–196, 1974.

Poster, C. K., Ultrasonic velocities in rocks from the Troodos massif, Cyprus, *Nature, 243,* 2–3, 1973.

Raitt, R. W., The crustal rocks, in *The Sea,* vol. 3, edited by M. N. Hill, pp. 85–102, John Wiley, New York, 1963.

Raitt, R. W., G. G. Shor, Jr., G. B. Morris, and H. K. Kirk, Mantle anisotropy in the Pacific Ocean, *Tectonophysics, 12,* 173–186, 1971.

Reinhardt, B. M., On the genesis and emplacement of ophiolites in the Oman Mountains' geosyncline, *Schweiz. Mineral. Petrogr. Mitt., 49,* 1–30, 1969.

Salisbury, M. H., and N. I. Christensen, The seismic velocity structure of a traverse through the Bay of Islands ophiolite complex, Newfoundland, an exposure of oceanic crust and upper mantle, *J. Geophys. Res., 83,* 805–817, 1978.

Shor, G. G., Jr., H. W. Menard, and R. W. Raitt, Structure of the Pacific basin, in *The Sea,* vol. 4, edited by A. E. Maxwell, pp. 3–27, John Wiley, New York, 1971.

Smewing, J. D., Mixing characteristics and compositional differences in mantle-derived melts beneath spreading axes: Evidence from cyclically layered rocks in the ophiolite of north Oman, *J. Geophys. Res., 86,* this issue, 1981.

Stern, C., M. J. de Wit, and J. R. Lawrence, Igneous and metamorphic processes associated with the formation of Chilean ophiolites and their implication for ocean floor metamorphism, seismic layering, and magnetism, *J. Geophys. Res., 81,* 4370–4380, 1976.

Sutton, G. H., G. L. Maynard, and D. M. Hussong, Widespread occurrence of a high-velocity basal layer in the Pacific crust found with repetitive sources and sonobuoys, in *The Structure and Physical Properties of the Earth's Crust, Geophys. Monogr. Ser.,* vol. 14, edited by J. G. Heacock, pp. 193–209, AGU, Washington, D. C., 1971.

Tippit, P. R., J. D. Smewing, and E. A. Pessagno, Jr., Biostratigraphy of sediments in the volcanic unit of the Samail ophiolite, *J. Geophys. Res., 86,* this issue, 1981.

Wenner, D. B., and H. P. Taylor, Jr., Oxygen and hydrogen isotope studies of the serpentinization of ultramafic rocks in oceanic environments and continental ophiolite complexes, *Am. J. Sci., 273,* 207–239, 1973.

(Received January 28, 1980;
revised May 21, 1980;
accepted July 2, 1980.)